ISSN 0915-633X

NATIONAL INSTITUTE FOR FUSION SCIENCE

3-Dimensional Simulation of Dynamo Effect of Reversed Field Pinch

S. Koide

(Received – Sep. 3, 1990)

NIFS-50 Sep. 1990

RESEARCH REPORT
NIFS Series

NAGOYA, JAPAN

3-Dimensional Simulation of Dynamo Effect of Reversed Field Pinch

Shinji Koide

National Institute for Fusion Science, Furou-cho, Chikusaku, Nagoya 464-01

Abstract

A non-linear numerical simulation of the dynamo effect of a reversed field pinch (RFP) with finite beta is presented. It is shown that the m=-1, n=(9, 10, 11,...., 19) modes cause the dynamo effect and sustain the field reversed configuration. The role of the m=0 modes on the dynamo effect is carefully examined. Our simulation shows that the magnetic field fluctuation level scales as $S^{-0.2}$ or $S^{-0.3}$in the range of $10^3 < S < 10^5$, while Nebel, Caramana and Schnack obtained the fluctuation level is independent of S for a pressureless RFP plasma.

Keywords: reversed field pinch(RFP), non-linear MHD simulation, dynamo effect, MHD fluctuation, finite beta.

§1. Introduction

The occurrence of large-scale magnetohydrodynamic (MHD) activity is commonly observed [1-6] in reversed field pinch (RFP) experiments. This activity, believed to be the manifestation of m=-1 tearing modes, has been linked to relaxation and configuration maintenance (the dynamo effect) [7-11] and may be responsible for the anomalous losses [8,11-14]. The presence of m=0 and $n \neq 0$ modes is also found in many experiments [2,4,13,14] and there is some controversy concerning the role of m=0 modes on the dynamo effect [15-17]

In this paper, we study the structure of the reversed field sustainment caused by the dynamo effect. The emphasis is to clarify the role that each tearing mode plays in the dynamo effect. We use a three-dimensional, semi-implicit, time-dependent, non-linear, compressible, resistive MHD simulation code. This code has been used to investigate field reversal sustainment by the dynamo effect due to the tearing and internal kink modes in an RFP [1]. Anomalous transport and current termination of an RFP has been simulated as well by this code [12,18,19]. Good correlation between simulation results and the experimental results of STP-3(M) is found.

The fluctuation level of MHD activities is important as the torchbearer of the dynamo effect in RFP. Strauss has shown that the $\delta B/B$ should scale as $S^{-1/3}$ for the RFP [20]. Nebel et al [17] found that $\delta B/B$ is independent of S, because of the fact that the m=-1 tearing mode resonances are far from the field reversal surface. Experimentally, relative magnetic-fluctuation amplitudes $\delta B/B$ roughly scale as $S^{-1/2}$ [2,13]. Our results indicate that for finite beta RFP, $\delta B/B$ scales as $S^{-0.1}$ or $S^{-0.15}$.

Regarding the role of the m=0 Fourier components in RFP dynamics, ref.16 reports the possibility of the RFP dynamo effect emerging as a nonlinearly driven m=0 reconnection. References 15,17 investigate the possibility of a phase shift between the m=-1 components of $\tilde{v} \times \tilde{B}$, resulting from couplings through the m=0 spectrum. These two papers 15.17 also

examine the internal electric field $E_{i\theta}$ at the field reverse surface. The positive internal electric field at the field reversal surface define the enhancement of the flux inside the reversal surface i.e. dynamo effect. We diagnose $E_{i\theta}$ at the reverse field surface as well as radial profile in order to obtain the radial profile of the dynamo. The role of each (m,n) mode on the dynamo effect is discussed with the simulation results.

This paper is organized as follows. In section 2, we describe the model of the MHD code. The results of the application of this code to RFP plasma are in Section 3. In section 4 we discuss the dynamo effect caused by MHD fluctuations. Section 5 contains the principal conclusion.

§2. Simulation Model

The code which we use is a three-dimensional, time-dependent, non-linear, compressible, resistive MHD simulation code in periodic cylindrical geometry. The normalized equations solved here are

$$\frac{\partial \vec{A}}{\partial t} = \vec{v} \times \vec{B} - \eta \vec{J} \ , \tag{2.1}$$

$$\rho \frac{D\vec{v}}{Dt} = -\vec{\nabla} p + \vec{J} \times \vec{B} + \frac{\nu}{S} \vec{\nabla}^2 \vec{v} \ , \tag{2.2}$$

$$\frac{Dp}{Dt} = -\frac{5}{3} p \vec{\nabla} \cdot \vec{v} + \eta J^2 + \kappa \nabla^2 p \ , \tag{2.3}$$

$$\vec{B} = \vec{\nabla} \times \vec{A} \ , \tag{2.4}$$

$$\vec{J} = \vec{\nabla} \times \vec{B} \ , \tag{2.5}.$$

$$\frac{D}{Dt} = \frac{\partial}{\partial t} + \vec{v} \cdot \vec{\nabla} \ , \tag{2.6}$$

where $\vec{B}$ is the magnetic field measured in units of a characteristic field $B_0 = B_z(r=0)$, length is measured in units of minor radius of the cylinder a, ρ is the mass density measured in units

of a characteristic density ρ_0, η is a nondimensional resistivity which is constant in time. $\vec{v}$ is the velocity measured in units of Alfven velocity $v_A=B_0/\sqrt{4\pi\rho_0}$, t is the time measured in units of Alfven transit time $\tau_A=a/v_A$, p is the thermodynamic pressure measured in units of $p_0=B_0^2/8\pi$, $\vec{A}$ is the vector potential measured in units of aB_0 and $\vec{J}$ is the current measured in units of B_0/a. To keep beta constant, the dissipation coefficient κ in the equation of pressure is feed-back controlled. The coefficient of viscosity ν is uniform in space and constant in time. According to ref. 21, the coefficient of viscosity ν is 2.5. We assume that the mass density is uniform in space and constant in time. S is the magnetic Reynolds or Lundquist number which is defined as $S=\tau_R/\tau_A$ where $\tau_R=4\pi a^2/\eta(0)$ is a characteristic resistive diffusion time.

These equations are solved using a Fourier expansion in the periodic poloidal and toroidal directions and a finite difference method in the radial direction with staggered meshes. The total mode number used here is 53. The radial mesh number is 200. Time advancement employs the implicit and semi-implicit method [22] which allows time steps orders of magnitude larger than those of a comparable explicit method.

The solutions of eqs.(2.1)-(2.3) are subject to perfect conducting wall boundary conditions, where total axial flux is constant in time. Further, we assume that total toroidal current is constant in time. The perfect conducting boundary condition and constant toroidal current imply that,

$$A_\theta = A_z = 0 \quad , \tag{2.7}$$

for $(m,n)\neq(0,0)$ modes and,

$$A_r = 0,\ A_\theta = \frac{\Phi}{2\pi} = const,\ \frac{\partial A_z}{\partial r} = -\frac{I_z}{2\pi} = const \quad , \tag{2.8}$$

for $(m,n)=(0,0)$ where Φ is the total flux of magnetic field and I_z is the z component of the total current.

The boundary conditions for the velocity and pressure are

$$v_r = 0, \quad p = 0. \tag{2.9}$$

For v_θ and v_z we use the free slip boundary conditions.

The equilibrium is modeled after Robinson's [23]. The magnetic field profiles of the initial equilibrium are obtained by giving the safety factor $q(r)=rB_z/RB_\theta$ and the Suydam parameter $C(r) = -\frac{4\pi p'}{rB_z^2}\left(\frac{q}{q'}\right)^2$;

$$q(r) = 0.1\left(1 - \frac{(R_s r)^2}{\alpha} - \frac{(R_s r)^4}{\lambda} - \frac{(R_s r)^6}{\delta} - \frac{(R_s r)^8}{\varepsilon} - \ldots\right) \tag{2.10}$$

$$C(r) = C(1 + c_1 r^{l_1} + c_2 r^{l_2})^{l_3} \tag{2.11}.$$

The Suydam stability condition is satisfied when $C(r)<1/8$. In this simulation, we choose realistic configurations with aspect ratio R/a being 5. Here R_s ,α,λ,δ,ε,C,c_1,c_2,l_1,l_2,l_3 are constant . We adopt R_s=4.2, α=10, λ=1/400, δ=-1/2450, ε=1/110000. It is assumed in this calculation that the initial distribution of the normalized resistivity is $\eta(r) = \frac{1}{S}\left|1 + (\eta_w^{1/2} - 1)r^{10}\right|^2$ and constant in time. The resistivity at the wall η_w is 10, Lundquist number S is between 10^3 and 10^5 and C for the initial profile is 0.1 and c_1,c_2,are both zero, corresponding to F= -0.44 and Θ =1.89

§3. The Simulation Results with Finite Beta

The initial equilibrium profiles of the toroidal and poloidal magnetic field B_z and B_θ, and the safety factor q given by eq.(2.10) and (2.11) are shown in Fig.1. In Fig.2, we show the time histories of parameters, F,θ,β,$q(0)$,Φ_v and $B_z(r=0)$ during the simulation where F,θ,β are defined by

$$F = \frac{B_{zw}}{\langle Bz \rangle} \tag{3.1}$$

$$\theta = \frac{B_{\theta w}}{\langle B_z \rangle} \tag{3.2}$$

$$\beta = \frac{\langle p \rangle}{\langle B^2 / 2\mu_0 \rangle}, \tag{3.3}$$

where B_{zw} , $B_{\theta w}$ are the mean z and θ components of the magnetic field at the wall, respectively. Brackets denote the average over the plasma. F maintains a negative value during the simulation. In the first stage, F increases and ,after t=150τ_A,decreases to - 0.4 at t=600τ_A. The θ value remains almost constant at 1.9. A feed back control of pressure keeps the β value constant (4%). In the first stage, $q(0)$ is almost constant, from 100τ_A to 250τ_A it falls to less than 0.1, after 250τ_A it fluctuates around 0.1. Φ_v is the axial magnetic flux inside the field-reversal surface defined by:

$$\Phi_v = \Phi(r_v) \quad ,$$

$$\Phi(r) = \int_0^r B_z^{00}(r')r'\mathrm{d}r' \ , \tag{3.4}$$

where supersubscript (00) means the (m,n)=(0,0) Fourier component of the quantity and r_v is the radius of the field-reversal surface. In the early stage, the flux Φ_v decreases due to finite resistivity , but after t=150τ_A it increases. The z component of magnetic field $B_z(0)$ at r=0 decreases as shown in Fig.2 . The time evolution of the q profile is shown in Fig.3. The location of the magnetic field reversal surface moves slightly throughout the simulation time. Outside the reversal surface, the q value decreases and inside the surface it increases after t= 300τ_A. The q value around the axis fluctuates and increases as a whole. This results from the fact that B_θ decreases. The temporal evolution of the mean parallel current λ profile, which is defined as

$$\lambda = \frac{\vec{J} \cdot \vec{B}}{B^2} \tag{3.5}$$

is shown in Fig.4. For r<0.4, the profile is flat ,which agrees with Taylor's theory [24]. The flattening of the parallel current by the dynamo modes in the plasma core is evident; the 'knee' in the profiles near r=0.5 corresponds to the location of the resonant surfaces of the most active dynamo modes (m=-1, n=9 to 19). The slope of λ (λ' is the driving term for tearing modes) is increased in the region between the reversal surface and the wall, but is relatively unaffected in the plasma core as mentioned in ref.25. In Fig.5. the energy in the radial component of the magnetic field of each (m,n) mode which is defined as

$$W_r^{m\,n} = \int (B_r^{m\,n})^2 \mathrm{d}^3 r \tag{3.6}$$

is plotted as a function of time, where the supersubscript (mn) means (m,n) Fourier component of the quantity. It is seen that the (-1,10) mode grows rapidly in the first stage. As shown in Fig.2, the resonance surface of the (-1,10) mode is near the axis in this first stage. After t=200τ_A, the (-1,10) mode is not resonant and its growth rate decreases. After t=300τA, (-1,10) mode decreases and other modes, for example (-1,9), (-1,11), etc. grow and then fluctuate. The m=0, $n\neq$0 modes increase after 220τ_A and fluctuate slowly. The value W_r^{0n} is small compared to m=-1 modes. The total energy in the radial component of the magnetic field,

$$W_r = \sum_{m,n} W_r^{m\,n} \tag{3.7}$$

fluctuates around a level W_{ra} during the saturation stage. The fluctuation magnetic energies during the simulated time interval are dominated by the (m=-1;n= 10, 11, 12,..... 19) modes. The n numbers included in m=0 modes are n=1,2,5. The magnetic energies of the other modes are much smaller than those of m=1 and m=0 modes.

The S dependence of the total magnetic energy in the radial component W_{ra} which is defined as the average of W_r after t=300τ_A is investigated. Fig.6 shows the S dependence of the fluctuation level for the 21 and 53 modes cases. The error bar is determined by the maximum and minimum value of W_r after t=300τ_A. The magnetic energy W_{ra} scales as $S^{0.2}$ to

$S^{-0.3}$ for both cases except for $S=10^3$. For the $S=10^3$ case, a large resistive dissipation makes MHD activity level small. In other numerical simulation, W_{ra} scales as $S^{-2/3}$ [20]. Nebel et.al. indicated that W_{ra} is independent of S according to their simulation, because of the fact that the m=-1 tearing mode resonances are far from the reversal surface [17]. Experimentally W_{ra} scales as S^{-1} [2,13]. Our result for the fluctuation level depends on S in contrast to Nebel et al's result., but the dependence is much weaker than the results of the experiments.

Now, we note the mode number convergence in these simulations for the case of $S=10^4$. Simulation with 63, 53 and 21 modes are performed and the time evolutions of the q profiles are shown in Fig.7. During a simulation with 21 modes, the q value near the edge changes rapidly from $300\tau_A$ to $400\tau_A$. Simulations with 53 and 63 modes,however, give a slower change. The history of the q profile for 53 is similar to that of 63 modes. This supports our choice of this mode number as being sufficient.

To understand the role of the m=0,$n\neq$0 mode, the case without these modes is simulated. The case without the m=0,$n\neq$0 modes time history of W^{mn} is shown in Fig.8 where W^{mn} is the magnetic field energy defined by

$$W^{mn}=\int (B^{mn})^2 d^3r. \tag{3.8}$$

The m=-1,n=10 mode is overpoweringly dominant. Comparing Fig.5 and Fig.8, it is clear that m=0,$n\neq$0 modes play the role of a mediator to the interaction of the m=-1 and high n modes. Figure 9 shows time histories of F, θ, β, $E_\theta^{00}(r_v)$ and Φ_v . It is seen that the field reversal is maintained even for this nearly single helicity case.

§4. MHD Fluctuations and Dynamo Effect

In this section the structure of the dynamo effect is studied. To understand the dynamo effect, we diagnose the internal electric field $E_{i\theta}$ defined by [26],

$$E_{i\theta}=\left(\vec{v}\times\vec{B}\right)_\theta^{00}=\left(v_z B_r - v_r B_z\right)^{00} \tag{4.1}$$

Ohm's law,

$$E_{\theta}^{00} = -E_{i\theta} + \eta J_{\theta}^{00} \tag{4.2}$$

and the Faraday equation give,

$$\frac{\partial \Phi}{\partial t} = E_{i\theta} - \eta J_{\theta}^{00} \tag{4.3}$$

The time rate of change of toroidal flux inside the field-reversal surface $r=r_v$ is determined by the mean poloidal internal electric field at the surface. If $E_{\theta}^{00}(r_v)>0$, the flux decreases; if $E_{\theta}^{00}(r_v)<0$, it increases. Since we assume that the total axial flux is conserved, the increase of Φ_v indicates field reversal maintenance.Under the action of resistive diffusion alone $E_{\theta}^{00}=\eta J_0>0$, the flux decays continuously. The presence of time-dependent magnetic fields may alter this picture. The second term of right hand side in eq. (4.3) describes the magnetic diffusion caused by resistive dissipation. The first term describes the dynamo or anti-dynamo effect.

The temporal evolution of the contribution of m=-1 each mode to the internal electric field $E_{i\theta}(m=-1,n)$ is shown in Fig.10 for the case of $S=10^4$. Each m=-1, n=(9,10,11, 12, ... 19) mode contributes to dynamo effect successively coincident with the rise and fall of the magnetic energies in each mode (see Fig.5) . There is a peak of each internal electric field between r=0.5 and field reversal surface. As n increases, the radius of the peak shifts towards the outer side. These m=-1 modes produce the continuous dynamo effect as a whole as shown in Fig.11(a). The m=0 mode contribution to $E_{i\theta}$ is rather complicated. The (0,0) mode contribution comes from the $v_r B_z$ term (note that $v_r^{00}\neq 0$ for the compressible plasma) and oscillates rapidly in time but in the average gives the anti-dynamo effect. The m=0, $n\neq 0$ modes contribution is $E_{i\theta}$ $(m=0,n\neq 0)$ <0 inside and $E_{i\theta}(m=0,n\neq 0)>0$ outside the reversal surface surface as shown in Fig.11(b). The $m\neq 0$ mode dynamo effect and the (0,0) mode anti-dynamo effect have about the same amplitude and set off but remain the $m\neq 0$ mode dynamo effect. The m=0, $n\neq 0$ dynamo effect is rather small for this $S=10^4$ case. The B_z field diffusion

term due to Joule dissipation is plotted in Fig.11(c). This is comparable to the total dynamo electric field. The summation produces the increase of F until t=150t_A, after that time the dynamo effect overcomes field diffusion.

The characteristics of the dynamo structure are influenced by the magnetic Reynolds number S. Fig.12 (a,b) compares the difference between a low S case (S=3x10^3) and high S case (S=10^5) at time t=500 τ_A. Since the field reversal sustainment is related to the internal electric field near the q=0 surface, we discuss the values around this surface. In the both cases the m=0,n=0 mode plays the role of an the anti-dynamo effect . At the field reversal surface, the mode has little effect on the anti-dynamo effect. The contribution of the m=-1 modes to the dynamo effect depends on S. For the low S case, the profile of the internal electric field caused by m=-1 modes $E_{i\theta}(m=-1)$ spreads out towards the outside of the field reverse surface. For the high S case, the profile is shallower and the absolute value decrease towards the field reverse surface. Hence the internal electric field $E_{i\theta}(m=-1)$ of the high S case is much less than that of the low S case. The profile and the magnitude of the m=0,$n\neq$0 modes $E_{i\theta}(m=0,n\neq0)$ look similar for the two different S. For the low S case, the m=-1 modes' contribution to the dynamo effect is dominant. For the high S case, the m=0,$n\neq$0 mode contributions to the dynamo effect become comparable with the m=-1, $n\neq$0 modes at least near the field reversed surface. It seems, indeed, remarkable that the m=-1 mode contribution to the dynamo effect is influenced by S.

§4. Conclusion

Three-dimensional numerical simulations of the non-linear interaction and evolution long wave-length modes in the RFP have been performed. We found that the total magnetic fluctuation field energy in the radial component of the modes scales as $S^{-0.2}$ or $S^{-0.3}$.This fluctuation scaling depends on the Lundquist number S and is stronger than the scaling of Nebel, Caramana and Schnack. However,it is weaker than the results from the experiments. The role of the m=0 and $n\neq$0 modes is only one of intermediary of the mode coupling for the low S case. Without the m=0 and $n\neq$0 modes, only a single mode grows and saturates. On the

other hand with the m=0 and $n\neq0$ modes, many modes grow and attenuate. We investigated the structure of the dynamo effect and the field reversal sustainment. The m=0, $n\neq0$ mode add little to the dynamo effect while the m=-1, $n\neq0$ mode is dominant for the low S case. For the high S case, the m=0,$n\neq0$ mode contributions to the dynamo become significant.

Acknowledgements

The author is very grateful to Professor T.Amano for helpful discussion and encouragement. He is grateful to Professor K.I.Sato and STP-3(M) group for helpful discussion and experimental suggestion. He acknowledges Dr. K.Urata for his help with the code .

References

1) K.I.Sato, T.Amano, Z.X.Chen, H.Arimoto, S.Yamada et al., in *Plasma Physics and Controlled Nuclear Fusion Research* (Proc. 11th Int. Conf. Kyoto,1986), vol.2,p413

2) T.Tamano, T.Carlstrom, C.Chu, R.Goforth, G.Jackson, R.La Haye, T.Ohkawa, M.Schaffer, P.Taylor, N.Brooks, R.Chase, in *Plasma Physics and Controlled Nuclear Fusion Research* (Proc. 9th Int. Conf. Baltimore,1982), vol.1,p609

3) H.A.B.Bodin, C.A.Bunting, P.G. Carolar, L.Giudicotti, C.W.Gowers, Y.Hirano, J.H.Hutchinson, P.A.Piotrowicz, T.Shimada, M.R.C.Warrs, in *Plasma Physics and Controlled Nuclear Fusion Research* (Proc. 9th Int. Conf. Baltimore ,1982), vol.1,p641

4) T.Shimada, Y.Yagi,Y.Hirano, Y.Hattori, I.Hirata, Y.Kondoh, Y.Maejima, K.Saito, S.Shiina, K.Ogawa, in *Plasma Physics and Controlled Nuclear Fusion Research* (Proc. 11th Int. Conf. Kyoto ,19), vol.2,p457

5) R.G.Watt and R.A.Nebel, Phys.Fluids 26(1983)1168

6) I.J.Hutchinson,M.Malacarne,P.Noonan, and D.Brotherton-Ratcliffe,

Nucl.Fusion 24(1984)59

7) N.Asakura, A.Fusisawa, T.Fujita, Y.Fukuda, et al., in *Plasma Physics and Controlled Nuclear Fusion Research* (Proc. 11th Int. Conf. Kyoto ,1987), vol.2,p433

8) D.D.Schnack,E.J.Caramana, and R.A.Nebel, Phys.Fluids 28(1985)321

9) E.J.Carramana, R.A.Nebel, D.D.Schnack, Phys. Fluids 26 (1983) 1305

10) H.R. Strauss, Phys.Fluids 27 (1984) 2580

11) Z.G. An, P.H. Diamond, R.D. Hazeltine, J.N. Leboeuf, M.N. Rosenbluth, R.D. Sydora, T.Tajima, B.A.Carreras, T.C. Hender, H.R. Hicks, J.A. Holmes, V.E. Lynch, and H.R. Strauss, in *Plasma Physics and Controlled Nuclear Fusion Research*, 1984, Proceedings of the 10th International Conference, London (IAEA, Vienna, 1985), Vol.2,p.231

12) T.S.Chen, T.Amano, Monte Carlo Studies of Transport in a Reversed Field Pinch, Rep. IPPJ-813 Nagoya University Institute of Plasma Physics(1987)

13) P.G.Carolan, B.Alper, M.K.Beveir, H.A.B.Bodin, C.A.Bunting, D.R.Brotherton-Ratcliffe, et al., in *Plasma Physics and Controlled Nuclear Fusion Research* (Proc. 10th Int. Conf. Vienma ,1985), vol.2,p449

14) K.I.Sato, K.Yokoyama, A.Nagata, S.Masamune, H.Arimoto, S.Yamada, A.Matsuoka, T.Tamaru, H.Oshiyama, Z.X.Chen, T.Amano, in *Plasma Physics and Controlled Nuclear Fusion Research* (Proc. 12th Int. Conf. Kyoto,1988), vol.2,p447

15) J.A.Holmes, B.A. Carreras, P.H.Diamond, and V.E.Lynch, Phys.Fluids 31(1988)1166

16) K.Kusano and T.Sato, Nucl.Fusion 27 (1987)821

17) R.A.Nebel, E.J.Caramana, and D.D.Schnack,Phys.Fluids B 1 (1989)1671

18) A.Nagata, H.Ashida, S.Koide, K.I.Sato, T.Amano, J.Phys.Soc.Jap.58(1989)3970

19) A.Nagata, S.Masamune, H.Arimoto, S.Yamada, K.I.Sato, T.Tamaru, Phys.Pluids B1(1989)2050

20) H.R.Strauss,Phys.Fluids 29(1985)3008

21) Y.L.Ho, S.C.Prager, D.D.Schnack, Phys Rev Lett 62(1989) 1504

22) D.D.Schnack, D.C.Baxter, E.J.Caramana, J. Comput. Phys 55 (1984) 485

23) D.C.Robinson: Nucl. Fusion 18(1978) 939

24) J.B.Taylor , in *Plasma Physics and Controlled Nuclear Fusion Research* (Proc. 5th Int. Conf. Tokyo,1974) vol.1,p161

25) D.D.Schnack, S.Ortolani, Nucl. Fusion 30 (1990) 277

26) R.T.Merrill, M.W.McElhinny: The Erthe's Magnetic Field (Academic press, New York, 1983) Chap.7, p231

Figure captions

Fig.1. The initial profile of $q(r)$, $B_\theta(r)$ and $B_z(r)$

Fig.2. Temporal evolution of F, θ, β, $q(0)$, Φ_v and $B_z(0)$

Fig.3. The temporal evolution of the mean safety factor profile $q=rB_z/RB_\theta$ for the case $S=10^4$.

Fig.4 The temporal evolution of the mean parallel current profile $\lambda = \frac{\bar{J}\cdot\bar{E}}{B^2}$ for the case $S=10^4$.

Fig.5. (a) Time evolution of the fluctuating magnetic energy in the radial component of m=-1,n=9,10,11 modes. The total fluctuation magnetic energy in the radial component saturates after $t=300\tau_A$.(b)Time evolution of the fluctuating magnetic energy in the radial component of m=-1,n=17,18,19 modes. (c)Time evolution of the fluctuating magnetic energy in the radial component of m=0, $n\neq0$ modes. The amplitudes are two orders of magnitude smaller than that of m=-1 modes.

Fig.6. The magnetic field total fluctuation energy level in the radial component W_{ra} vs Lundquist number S for the case of 21 and 53 modes. The fluctuation level scales as as $S^{-0.2}$ or $S^{-0.3}$.

Fig.7. The mode convergence test for 21, 53, 63 modes cases. The time evolution of q profiles are compared. Good agreement is found between the 53 and 63 modes simulation.

Fig.8. Time evolution of the fluctuating total magnetic energy and that of dominant modes for the case without m=0,$n\neq0$ modes.

Fig.9. The time evolution of F, θ, β, internal electric field at the field reversal surface $E_\theta^{00}(r_v)$ and the toroidal flux inside the surface Φ_v (without m=0,$n\neq0$ modes) The temporal evolution of F and Φ_v indicate the field reversal sustainment.

Fig.10. The m=-1 modes contribution profile to the dynamo effect versus time.

Fig.11 (a) The m=-1 modes contribution profile to the internal electric field $E_{i\theta}(m=-1)$ versus time. (b) The m=0, $n\neq 0$ modes contribution profile to the internal electric field $E_{i\theta}(m=0,n\neq 0)$ versus time. (c) The resistive dissipation profile versus time.

Fig.12 (a) Internal electric fields and resistive diffusion for $S=3\times10^5$ at $t=500\tau_A$

(b) Internal electric fields and resistive diffusion for $S=10^5$ at $t=500\tau_A$.

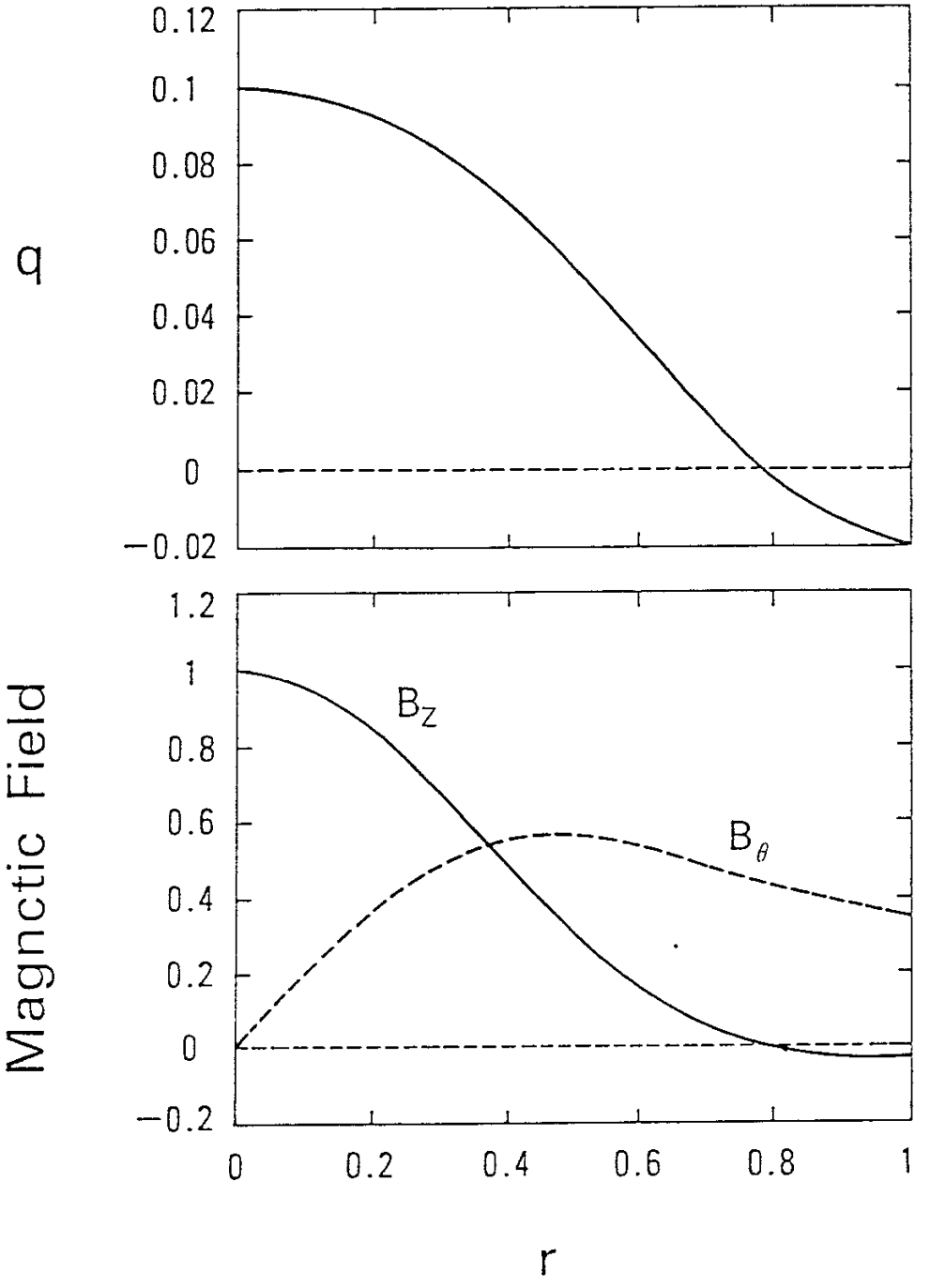
q
0.12
0.1
0.08
0.06
0.04
0.02
0
−0.02
Magnctic Field
1.2
1
0.8
0.6
0.4
0.2
0
−0.2
B_z
B_θ
0
0.2
0.4
0.6
0.8
1
r

Fig.1

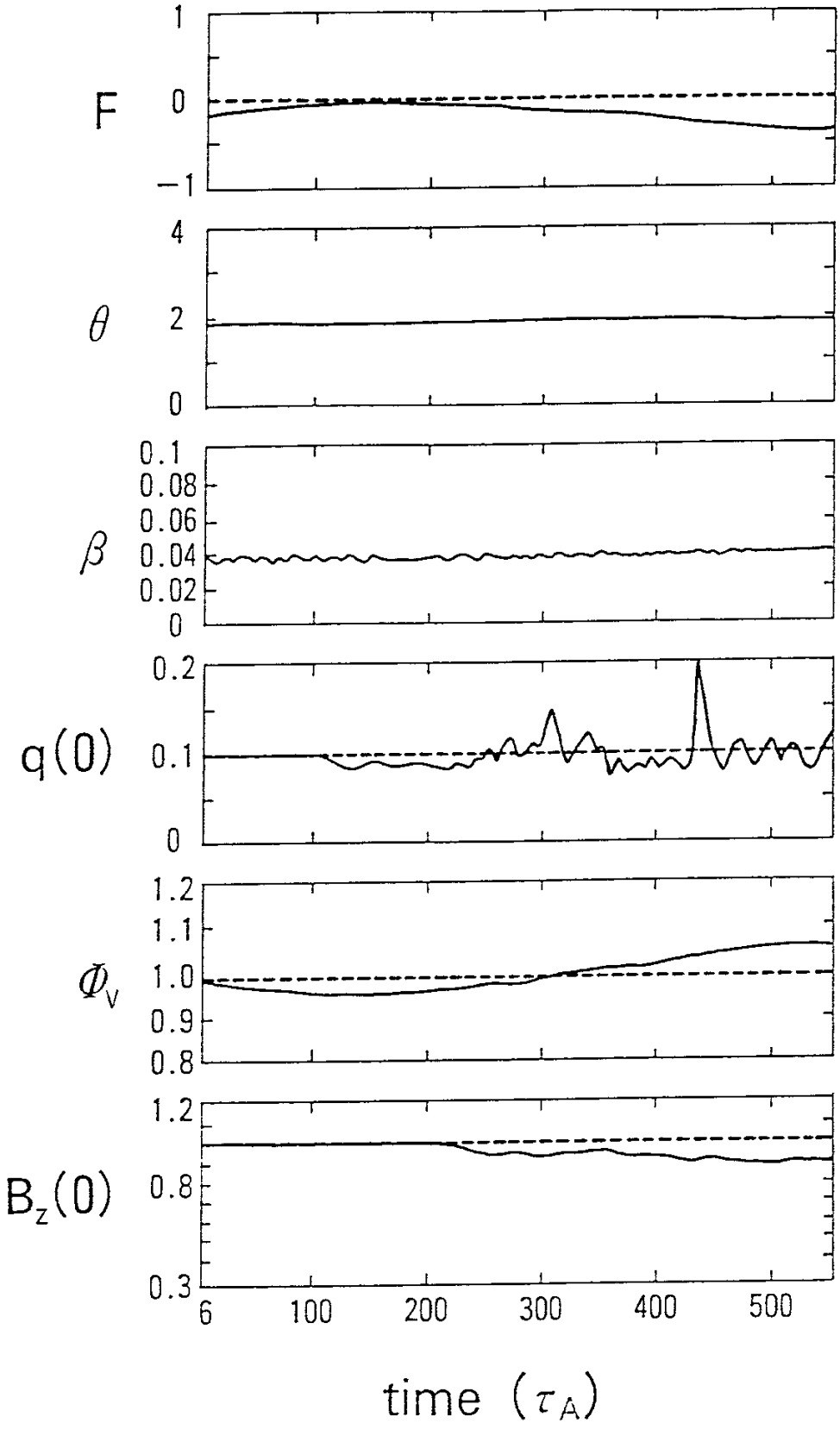
F
1
0
−1
θ
4
2
0
β
0.1
0.08
0.06
0.04
0.02
0
q(0)
0.2
0.1
0
Φv
1.2
1.1
1.0
0.9
0.8
Bz(0)
1.2
0.8
0.3
6
100
200
300
400
500
time (τA)

Fig.2

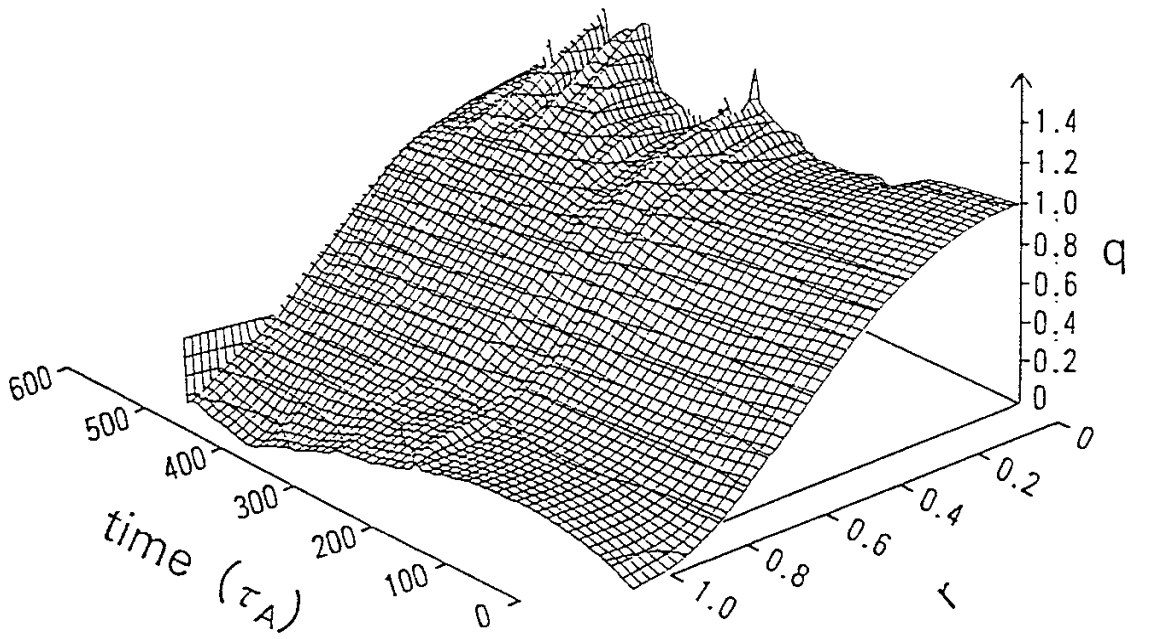
600
500
400
300
200
100
0
time (τ_A)
1.0
0.8
0.6
0.4
0.2
0
r
1.4
1.2
1.0
0.8
0.6
0.4
0.2
0
q

Fig.3

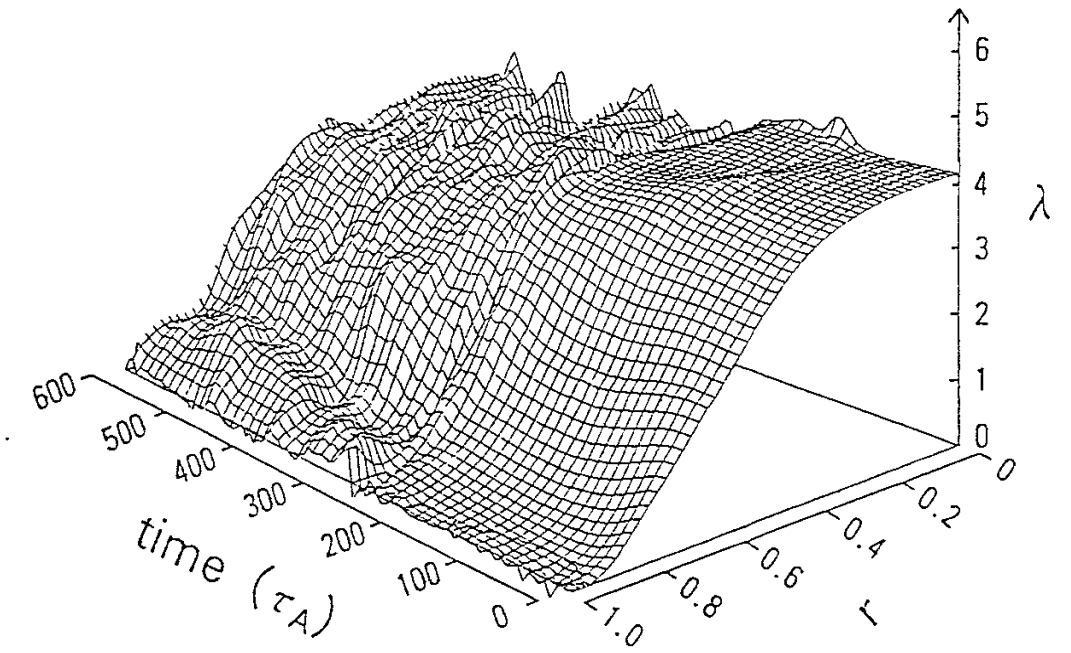

Fig.4

(a)

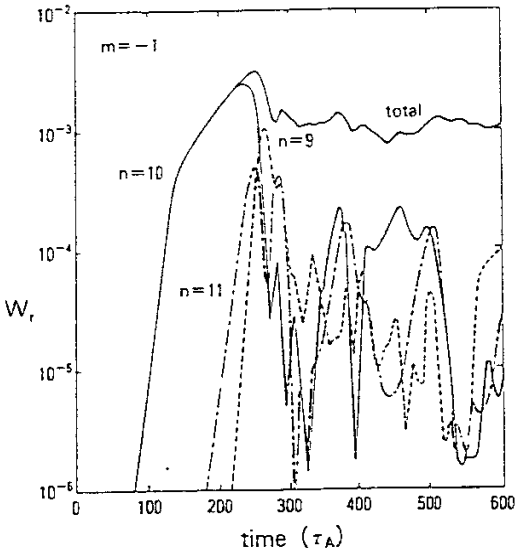
m=−1
total
n=9
n=10
n=11
W_r
time (τ_A)

(b)

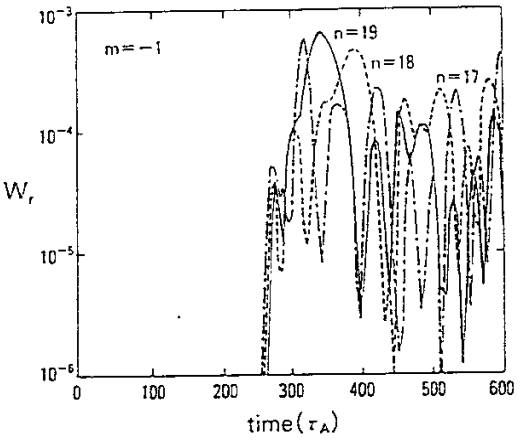
m=−1
n=19
n=18
n=17
W_r
time(τ_A)

(c)

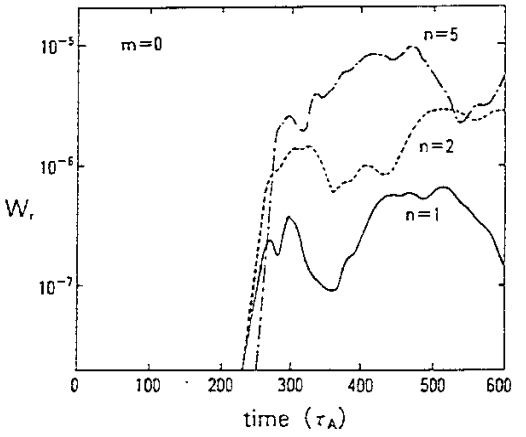
m=0
n=5
n=2
n=1
W_r
time (τ_A)

Fig.5

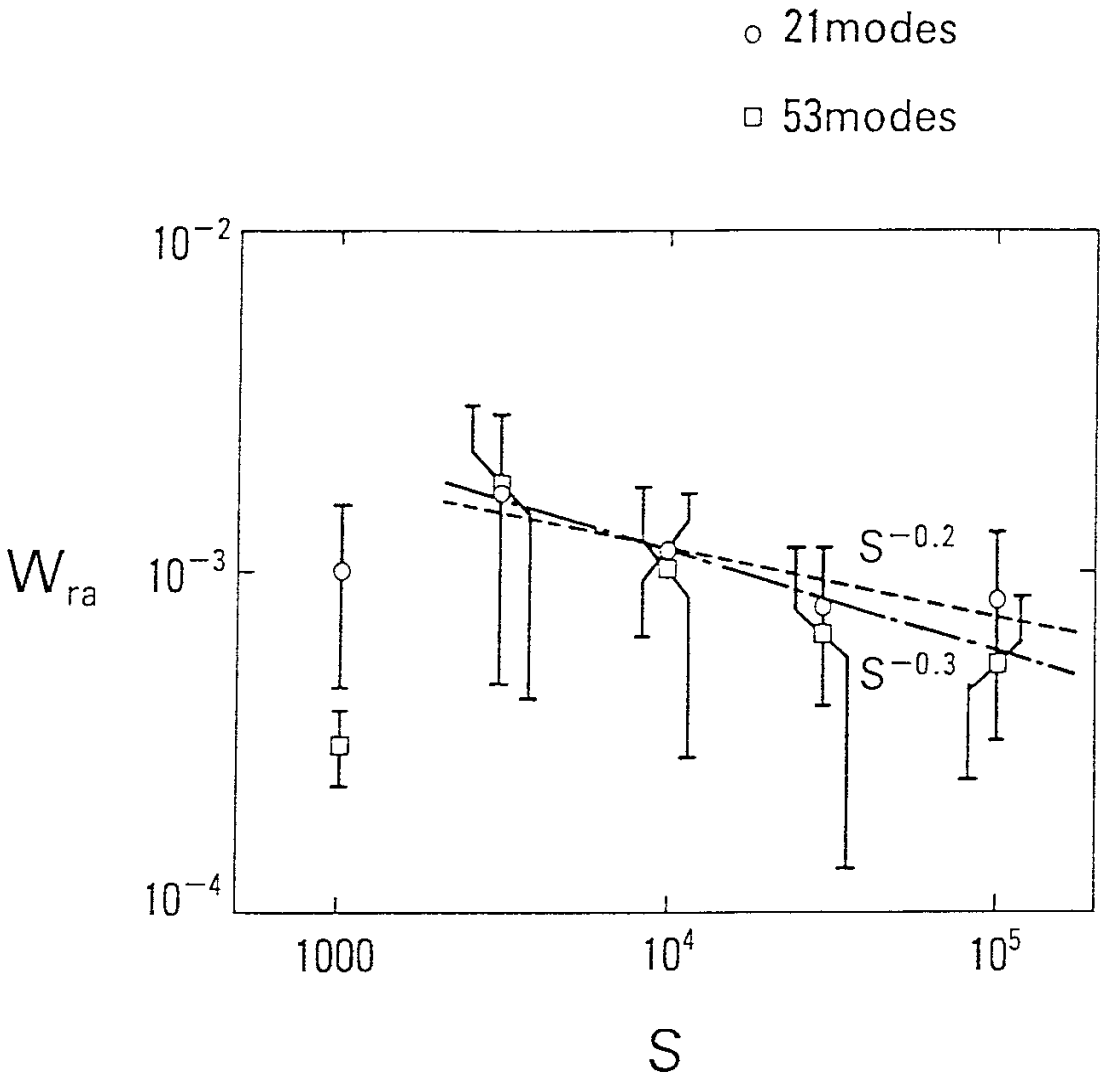

Fig.6

(a) 21modes

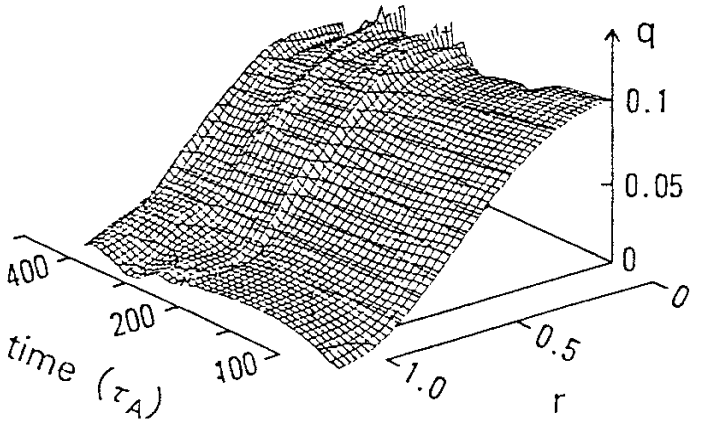

(b) 53modes

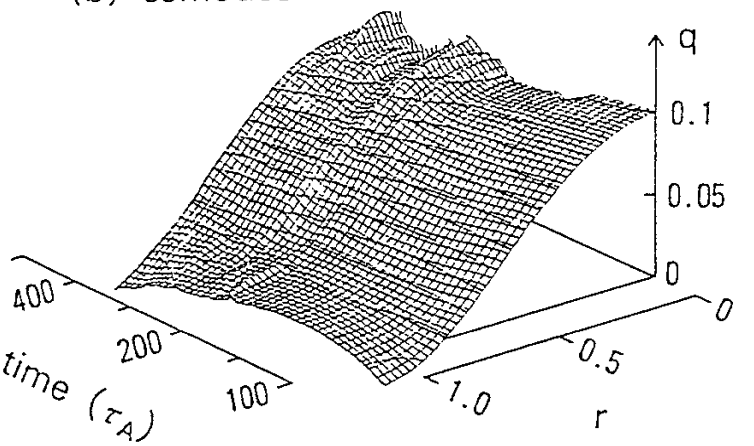

(c) 63modes

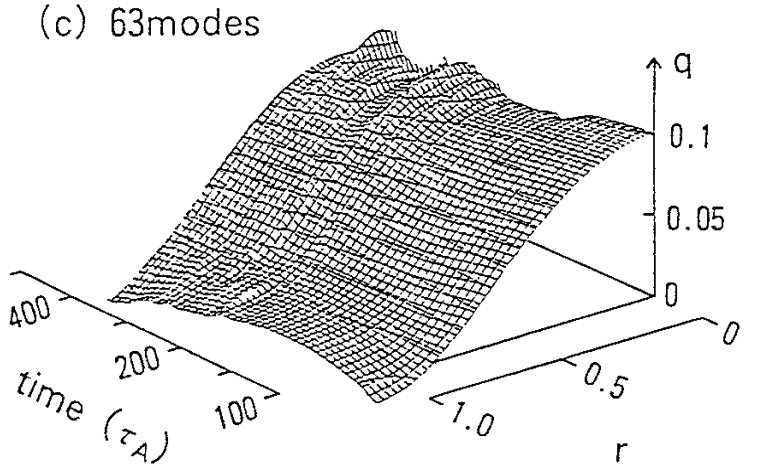

Fig.7

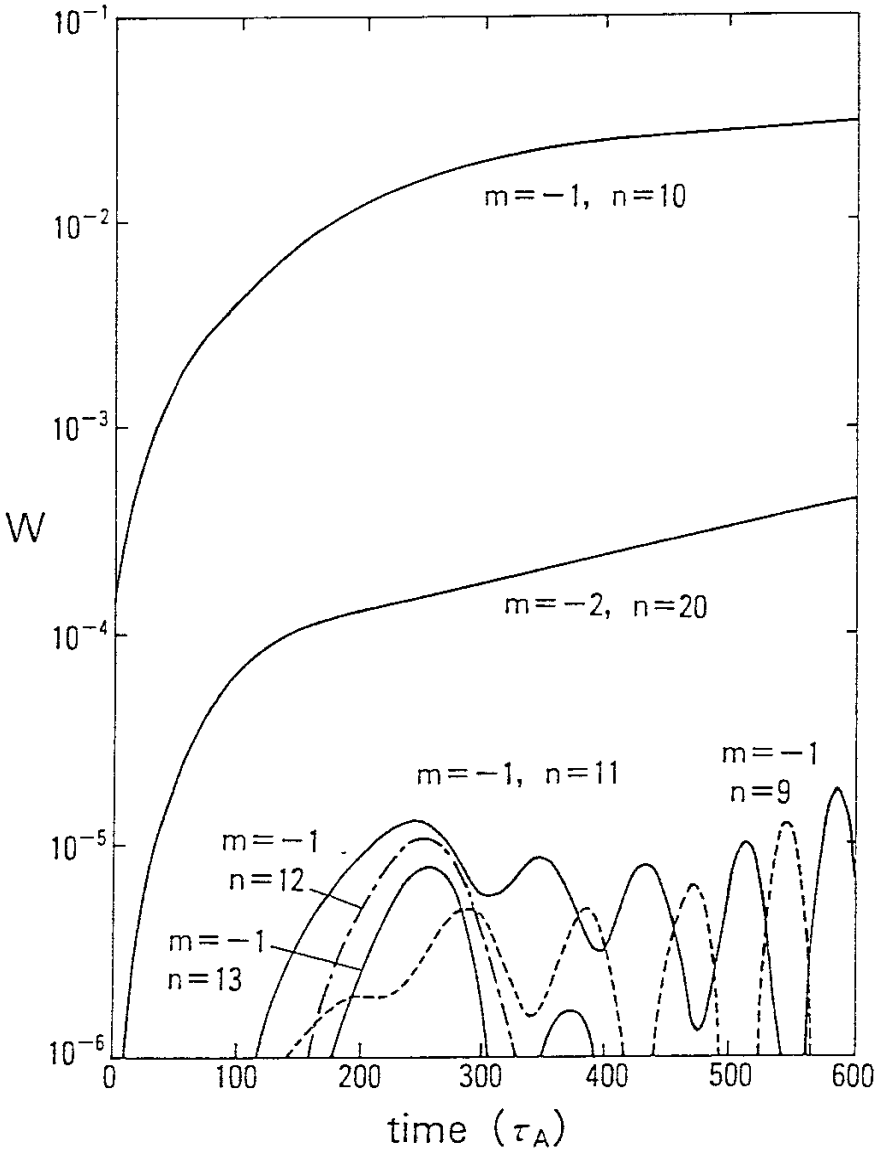
10^{-1}
10^{-2}
10^{-3}
10^{-4}
10^{-5}
10^{-6}
W
m=−1, n=10
m=−2, n=20
m=−1, n=11
m=−1
n=9
m=−1
n=12
m=−1
n=13
0
100
200
300
400
500
600
time (τ_A)

Fig.8

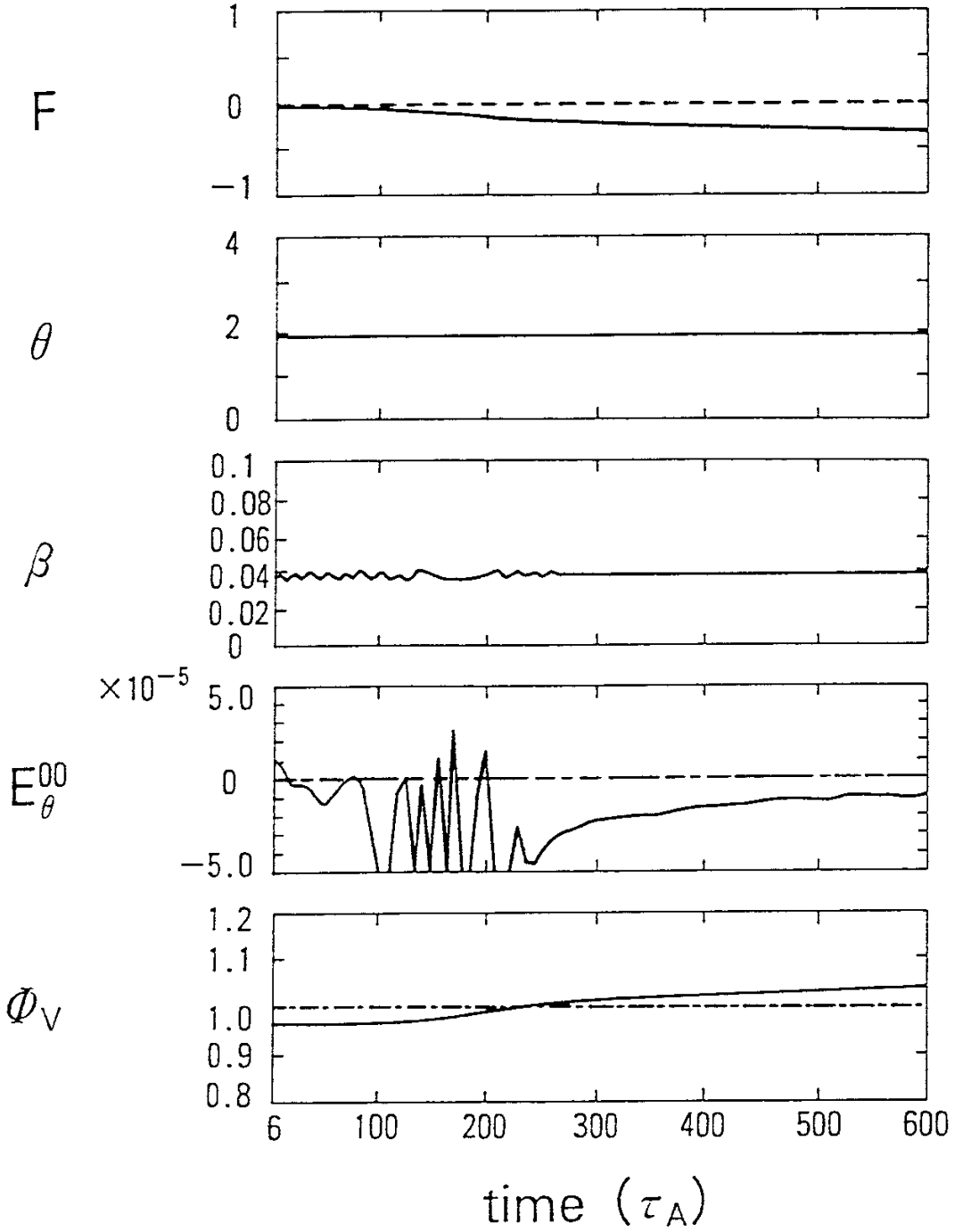
F
1
0
−1
θ
4
2
0
β
0.1
0.08
0.06
0.04
0.02
0
×10−5
E00θ
5.0
0
−5.0
Φv
1.2
1.1
1.0
0.9
0.8
6
100
200
300
400
500
600
time (τA)

Fig.9

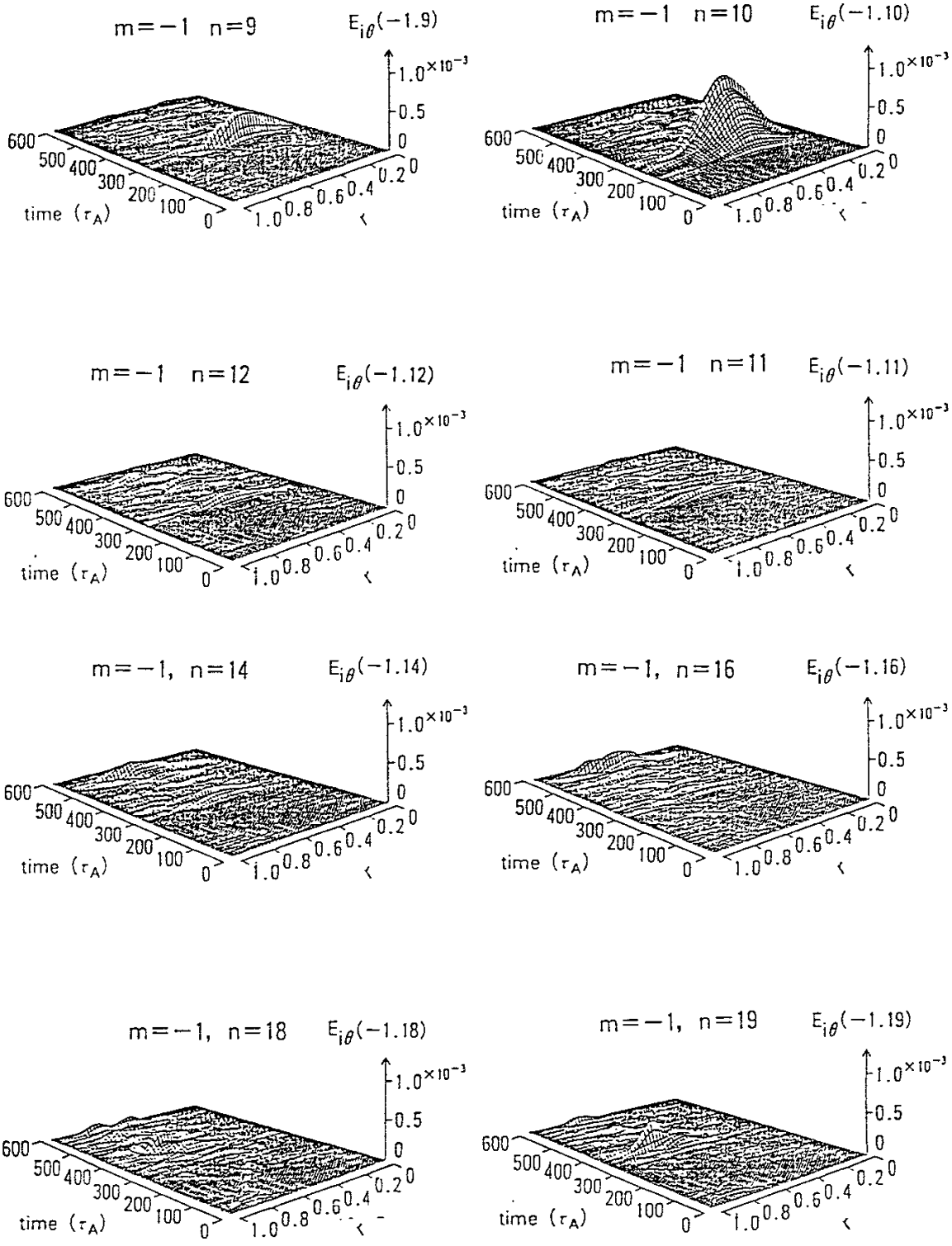
m=−1 n=9 $E_{i\theta}(-1.9)$
m=−1 n=10 $E_{i\theta}(-1.10)$
m=−1 n=12 $E_{i\theta}(-1.12)$
m=−1 n=11 $E_{i\theta}(-1.11)$
m=−1, n=14 $E_{i\theta}(-1.14)$
m=−1, n=16 $E_{i\theta}(-1.16)$
m=−1, n=18 $E_{i\theta}(-1.18)$
m=−1, n=19 $E_{i\theta}(-1.19)$
1.0×10^{-3}
0.5
0
time (τ_A)
600
500
400
300
200
100
0
1.0
0.8
0.6
0.4
0.2
0
r

Fig.10

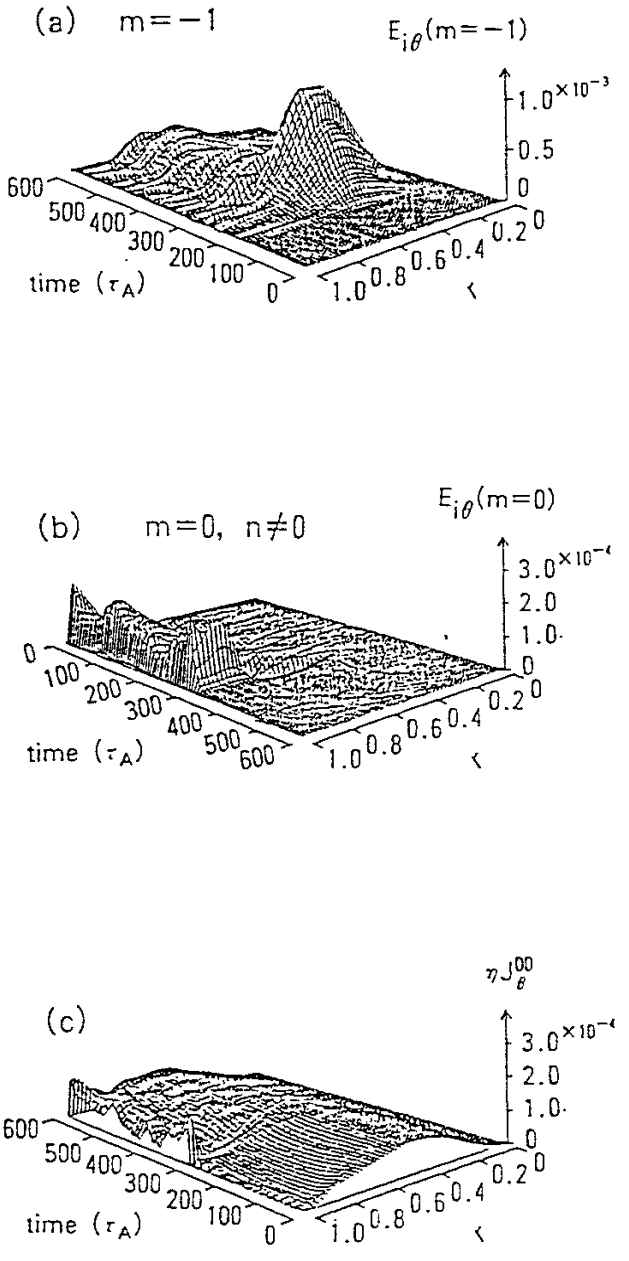
(a) m=−1
$E_{i\theta}$(m=−1)
1.0×10⁻³
0.5
0
600
500
400
300
200
100
0
time (τ_A)
0
0.2
0.4
0.6
0.8
1.0
r
(b) m=0, n≠0
$E_{i\theta}$(m=0)
3.0×10⁻⁴
2.0
1.0
0
0
100
200
300
400
500
600
time (τ_A)
0
0.2
0.4
0.6
0.8
1.0
r
(c)
ηJ_θ^{00}
3.0×10⁻⁴
2.0
1.0
0
600
500
400
300
200
100
0
time (τ_A)
0
0.2
0.4
0.6
0.8
1.0
r

Fig.11

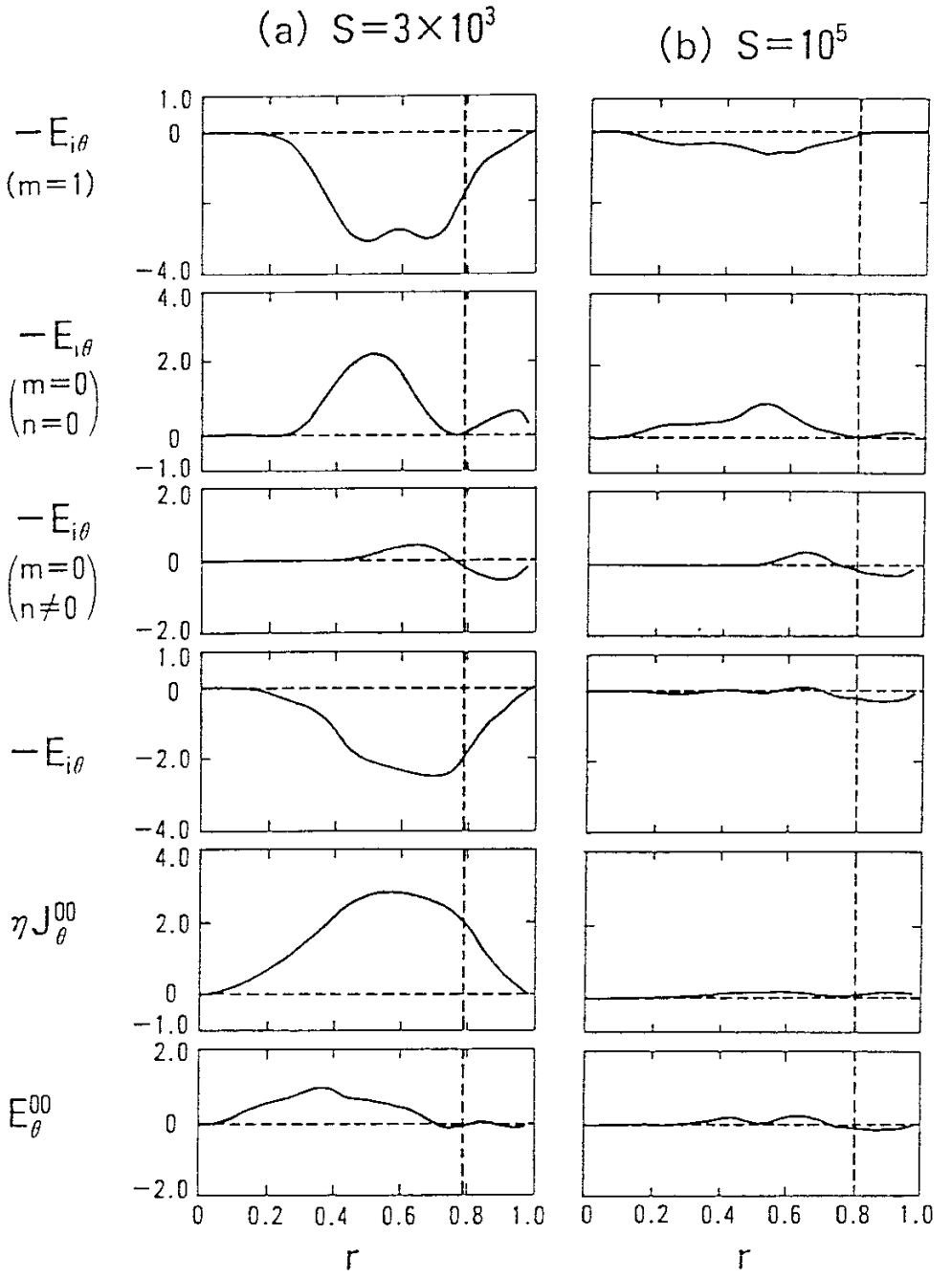
(a) S=3×10³
(b) S=10⁵
−Eiθ (m=1)
−Eiθ (m=0, n=0)
−Eiθ (m=0, n≠0)
−Eiθ
ηJθ00
Eθ00
1.0
0
−4.0
4.0
2.0
0
−1.0
2.0
0
−2.0
1.0
0
−2.0
−4.0
4.0
2.0
0
−1.0
2.0
0
−2.0
0 0.2 0.4 0.6 0.8 1.0
r

Fig.12